ELECTRICAL AND DIELECTRIC PROPERTIES OF RUBBER

C. M. ROLAND

NAVAL RESEARCH LABORATORY, CHEMISTRY DIVISION, CODE 6105, WASHINGTON DC 20375

ABSTRACT

This review describes electrical and dielectric measurements of rubbery polymers. The interest in the electrical properties is primarily due to the strong effect of conductive fillers, the obvious example being carbon black. Conductivity measurements can be used to probe dispersion and the connectivity of filler particles, both of which exert a significant influence on the mechanical behavior. Dielectric relaxation spectra are used to study the dynamics, including the local segmental dynamics and secondary relaxations, and for certain polymers the global chain modes. A recent development in the application of nonlinear dielectric spectroscopy is briefly discussed. [doi:10.5254/rct.15.84827]

CONTENTS

I. INTRODUCTION

The mechanical, rheological, and many other physical properties of polymers reflect the underlying dynamics of the chains and chain segments. Theses dynamics, in turn, are governed by the chemical structure and any fillers present in the compound. Experimental methods to study relaxation phenomena in polymers span a variety of techniques, including quasi-elastic neutron and light scattering, NMR, and mechanical and dielectric spectroscopies. The wide range of frequencies probed by dielectric spectroscopy, from milli- to gigahertz, makes it an especially attractive method. The enormous size of macromolecules, which can be two orders of magnitude larger than the distance between segments, gives rise to motions spanning an enormous range of time scales, necessitating broadband measurements. Electrical and dielectric methods are also used to characterize reinforcement of polymers, since important fillers such as carbon black and carbon-based nanoparticles are electrically conductive.

II. EXPERIMENTAL METHODS

A. ELECTRICAL CONDUCTIVITY

According to Ohm's law, in the linear regime the steady-state electric current is proportional to the electric potential (voltage), with the proportionality factor termed the conductance, G. Thus, a

*Corresponding author. Ph: 202-767-1719; email: roland@nrl.navy.mil

simple direct current (dc) resistance measurement can be used to determine the conductivity of a material. The International System of Units unit for G is the siemen (S). Since the reciprocal of G is the resistance, R, 1 S = 1 reciprocal ohm (or mho). The material property that is independent of the dimensions of the conductor is the conductivity, σ, given by the product of G and the cross-sectional area, A, divided by the length, d, of the conductor; σ has units of siemens per meter.

In addition to electrical conduction, polymers often contain mobile ions, such as electrolytic impurities, whose diffusion constitutes another means of charge transport, the ionic conductivity, σ_{ion}. Since σ_{ion} is unrelated to filler structure (although filler particles can introduce ionic species to the material), its measurement is usually part of electrochemical experiments or less often relaxation studies. The latter comes from the fact that ion mobility is coupled to the polymer segmental dynamics, as motion of the repeat units opens pathways for ion diffusion. At high frequencies local excursions and vibrations of ions also contribute to the conductivity, but only to the frequency-dependent (alternating current [ac]) component. For the analysis of the connectivity of carbon black and other conductive fillers, it is usually sufficient to measure the dc-conductivity. This frequency-independent conduction arises from independent diffusion of the charges; only at higher concentrations do these motions become correlated, requiring ac experiments. However, even if the conductivity does not change with frequency, dc measurements can be sensitive to drift and background currents, whereas ac measurements can circumvent these sources of error. The ac-conductivity, $\sigma^*(\omega)$, is a frequency-dependent, complex quantity. Its reciprocal is the impedance, $z^*(\omega)$. Impedance spectroscopy is applied to the study of conduction, including the transport and adsorption of electrons or ions, and to electrochemical processes. Analogous to Ohm's law, the complex impedance is given by the ratio of the applied voltage (which is constant for dc measurements) and the current; $z^*(\omega)$ has the unit of ohm. If the sample under test and the associated cabling have negligible capacitance, C, and inductance, then $R = z$; otherwise, the resistance can be obtained from the high-frequency limiting value of the real part of the impedance

$$R = \lim_{\omega \to \infty} z'(\omega) \tag{1}$$

The impedance is related to the dielectric permittivity, $\varepsilon^*(\omega)$, as

$$\varepsilon^*(\omega) = \left(i\omega z^*(\omega) C_0 \right)^{-1} \tag{2}$$

with C_0 the capacitance of a vacuum and $i = \sqrt{-1}$. The dc-conductivity can be obtained from the permittivity by using

$$\varepsilon_{dc}^*(\omega) = \frac{\sigma^*(\omega)}{i\omega\varepsilon_0} \tag{3}$$

in which ε_0 is the permittivity of vacuum ($= \frac{d}{A} C_0 = 8.854$ pF/m). Usually the dc-conductivity of polymers exhibits power-law behavior

$$\varepsilon_{dc}^*(\omega) = \frac{\sigma_{dc}}{\varepsilon_0 (i\omega)^j} \tag{4}$$

with the exponent j (≤ 1) equal to unity for free conduction.

The permittivity is a compliance, reflecting the polarization at constant electric field; the corresponding dielectric modulus, which is the polarization at constant charge, is related as

$$M^*(\omega) = 1/\varepsilon^*(\omega) \tag{5}$$

Although the two representations contain the same information, an advantage of the modulus function is that the conductivity manifests as a peak in the dielectric loss modulus, $M''(\omega)$. The
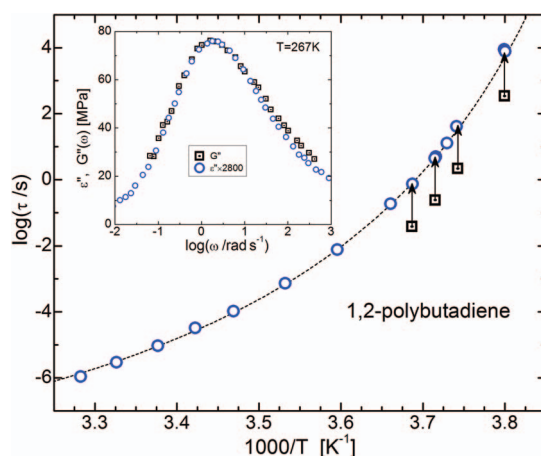
FIG. 1. — Local segmental relaxation times of 1,2-polybutadiene from the peak in the mechanical loss modulus (squares) and in the dielectric loss (circles). The arrows represent a shift by a factor of 20, to indicate the comparable temperature dependence of the τ_α. The inset shows representative spectra; the dielectric peak was shifted horizontally and multiplied by the indicated factor to superpose the peak maxima. Data from ref 7.

inverse of the frequency of this peak defines a conductivity relaxation time, although this is phenomenological and lacks physical significance (e.g., it is not related to an ion hopping time).

B. DIELECTRIC LOSS

The most commonly observed peaks in dielectric loss spectra are due to motion of the molecules or polymer chains, primarily reorientations of segments or moieties having a nonzero dipole moment, μ. There is an inflection in the real part of the permittivity corresponding to a peak in $\varepsilon''(\omega)$ (see Eq. 9). Using modern dielectric instruments, polymers with very weak dipole moments ($\mu < 0.05$ D per repeat unit) can be measured; examples include atactic polypropylene[1] and polyisobutylene.[2] Dielectric relaxation measurements almost always use weak electric fields, so there is no net polarization of the sample. Any orientation induced in the dipoles is overcome by thermal agitation, and the material remains isotropic. This is the typical linear experiment that enables study of the equilibrium dynamics.

The absorption of electrical energy is maximal when the frequency of the electric field and that of the dynamics coincide, so that the inverse frequency of the maximum in $\varepsilon''(\omega)$ defines the relaxation time, τ_α. The subscript α denotes that this is the longest relaxation time (lowest frequency), corresponding to the local segmental dynamics of polymers. (Polymers with a dipole moment parallel to the chain contour have a lower frequency dispersion in their spectrum, arising from fluctuations in the chain end-to-end vector (see Section III.B.4). The τ_α designation is nonetheless retained for the segmental relaxation time.)

Although in principle dielectric and dynamic mechanical spectra reflect the same motions of the chains and chain segments, there are differences in both the intensities and frequencies of the respective peaks.[3–5] The exact relationship between the two measurements is complex, depending inter alia on the respective relaxation strengths.[6] Figure 1 shows that the temperature dependences of the local segmental relaxation times for 1,2-polybutadiene from dynamic mechanical and from dielectric spectroscopy are equivalent.[7] And as seen in the inset, the dispersions in the loss spectra are similar, although the mechanical loss is a modulus and the dielectric loss is a compliance (making τ_α for the latter a bit longer). The advantage of dielectric experiments is that they are
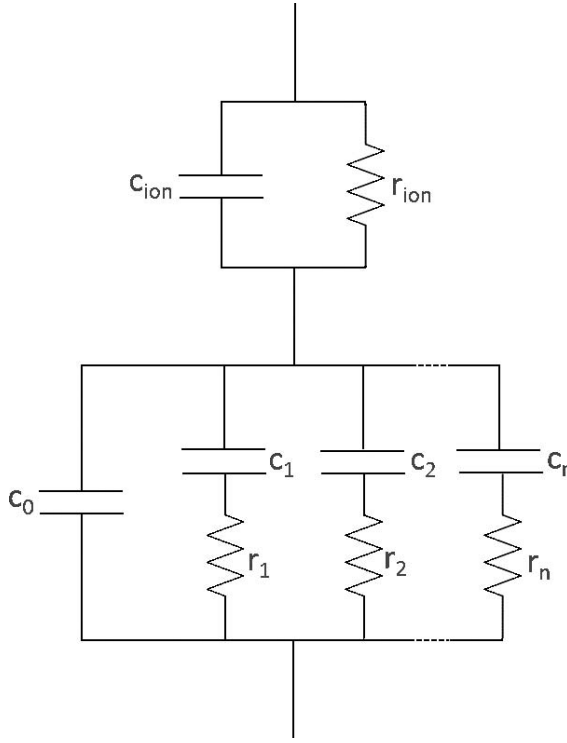
FIG. 2. — Equivalent circuit diagram for a viscoelastic response described by exponential decays coupled in parallel and an ionic conductivity in series. Symbols c_i and r_i represent capacitors and resistors, respectively.

broadband (routinely 10^{-4}–10^6 Hz) and amenable to measurements at elevated pressure (up to 6 GPa has been reported[8]). Unlike conductivity data, relaxation spectra are invariably expressed in the permittivity representation, rather than using impedance functions. The interpretation of relaxation spectra is through comparison to models for the dynamics, whereas impedance spectroscopy measurements generally rely on equivalent circuits for analysis. Formally, relaxation spectra can be described in terms of a distribution of exponential relaxation processes,[9,10] so that an equivalent circuit diagram[11] can be constructed (Figure 2). This representation is a mathematical convenience, and its successful fitting to experimental data does not guarantee that the molecular motions underlying the relaxation spectra are actually a collection of exponential decays.[3,12]

A large contribution to the permittivity from mobile ions in the material can mask relaxation peaks in the dielectric loss, especially toward lower frequencies. According to the Kramer–Kronig formula

$$\varepsilon'(\omega) = \varepsilon_\infty + \frac{2}{\pi} \int_0^\infty \varepsilon''(\omega_0) \frac{\omega_0}{\omega_0^2 - \omega^2} d\omega_0 \qquad (6)$$

and

$$\varepsilon''(\omega) = \frac{\sigma_{dc}}{\varepsilon_0 \omega} + \frac{2}{\pi} \int_0^\infty \varepsilon'(\omega_0) \frac{\omega_0}{\omega_0^2 - \omega^2} d\omega_0 \qquad (7)$$

showing that the dc-conductivity makes no contribution to the real part of the permittivity. Thus, when intense conductivity masks a relaxation peak of interest, Eq. 7 can be used to obtain the

dielectric loss *sans* the conductivity term

$$\varepsilon''_{KK}(\omega\ ) = \frac{2}{\pi} \int_0^\infty \varepsilon'(\omega_0) \frac{\omega_0}{\omega_0^2 - \omega^2} d\omega_0 \tag{8}$$

More often an approximation to Eq. 8 is applied, which is almost quantitative for broad relaxation peaks[13]

$$\varepsilon''_{KK}(\omega\ ) \approx -\frac{\pi}{2} \frac{\partial \varepsilon'(\omega)}{\partial \ln\omega} \tag{9}$$

Relaxation spectra calculated by Eq. 9 are narrower than directly measured $\varepsilon''(\omega)$, although the frequencies of the peak maxima, and thus the relaxation times, are the same. This derivative analysis can also be used to shift the effect of electrode polarization away from the main relaxation.[14]

C. USE OF IMPEDANCE FUNCTION IN DIELECTRIC RELAXATION EXPERIMENTS

Dielectric relaxation measurements to determine the dynamics of polymers and liquids analyze the permittivity, rather than the impedance representation used, inter alia, for conductivity studies. However, when measurements are extended to high frequencies, which for a typical dielectric relaxation experiment are defined as frequencies beyond $\sim 10^6$ Hz, the complex impedance can be used to remove the effects of the resistance and inductance of the electrical cables connecting the sample electrodes to the analyzer. The resistance is given by Eq. 1 and the equation for the inductance, L, or resistance due to current changes in the cable and a consequent time-dependent magnetic field, is

$$z''(\omega) = \frac{\kappa}{\omega} - \omega L \tag{10}$$

where κ is a constant. The measured impedance functions can then corrected to yield spectra free from these cable effects

$$z'_{corr}(\omega) = z'(\omega) - R \tag{11}$$

and

$$z''_{corr}(\omega) = \omega L z''(\omega) \tag{12}$$

In turn, the permittivity is calculated from the corrected impedances using Eq. 2.

To apply Eqs. 1 and 10 requires dielectric measurements that are free from relaxation peaks, that is, any capacitance changes due to the sample. This can be done by measurements at temperatures well below the glass transition temperature, T_g, as illustrated in Figure 3 for a crosslinked 1,2-polybutadiene. The polymer has a small dipole moment; hence, the cable interferences show up at relatively low frequencies, ~ 3 kHz. The fit to the real and imaginary impedance functions yields R and L, respectively, for the cable assembly. Equations 11 and 12 are then used to calculate the corrected impedance functions, from which the permittivity is obtained via Eq. 2. The removal of the cable effects enables determination of the actual material response (Figure 3).[15]
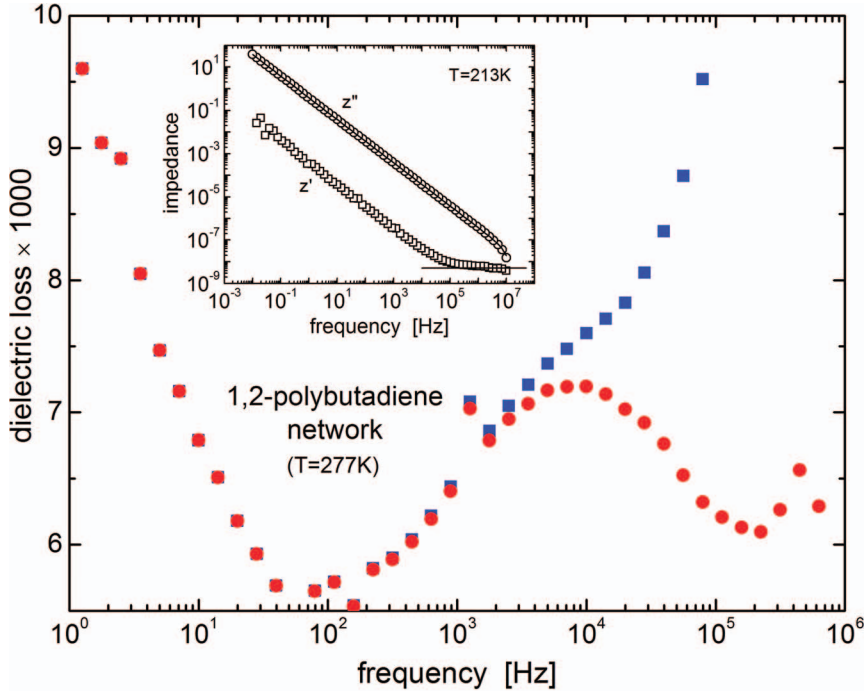
FIG. 3. — (Inset) Real and imaginary permittivity measured for a crosslinked rubber at a temperature sufficiently low that no relaxation processes are present in the spectra. The solid lines are the fits of Eq. 1 to z' at high frequencies and of Eq. 10 to z''. (Main) Dielectric loss spectrum of the network at a temperatures 5 K below T_g. The rise at high frequencies in the measured spectra (squares) is due to the cables; after correction the actual secondary loss peak is obtained (circles). The rise at low frequencies is due to the local segmental relaxation process. Data from ref 15.

III. APPLICATIONS TO RUBBER

A. ELECTRICAL CONDUCTIVITY OF FILLED RUBBER

Generally polymers have low electrical conductivity, for common gum rubbers falling in the range 10^{-9}–10^{-15} S/m. This contrasts with the relatively high conductivity of carbon black (10^4–10^5 S/m), resulting from the graphitic layers providing delocalized "mobile" π-electrons. Thus, addition of carbon black or other conductive fillers increases σ_{dc} by as much as several orders of magnitude when the volume fraction of particles, ϕ, becomes sufficient to yield continuous connections (Figure 4).[16] A connected particle network enhances conductivity by two mechanisms: conventional ohmic contacts, for which the resistance is inversely proportional to the square root of the contact area between the particles,[17] and tunneling. Tunneling is a quantum mechanical phenomenon in which a nonzero wave probability enables an electron to pass through a barrier that would be insurmountable classically. Quantum tunneling is significant for barrier thicknesses of a couple nanometers or smaller, becoming the dominant conduction mechanism when an insulating layer exists between the surface of the particles (due, for example, to bound rubber or an oxide layer) or when the particle separation is nonzero.

Percolation refers to the state of particle interconnectedness at which continuous paths span representative volume elements.[18,19] Well above the threshold concentration for percolation, ϕ^*, σ becomes essentially invariant to filler content.[20] This corresponds to the formation of a three-dimensional "skeleton" of conductive particles. As an example, for spherical particles with simple cubic packing, sufficient conductive pathways are present at $\phi = 0.52$ for the effect of filler
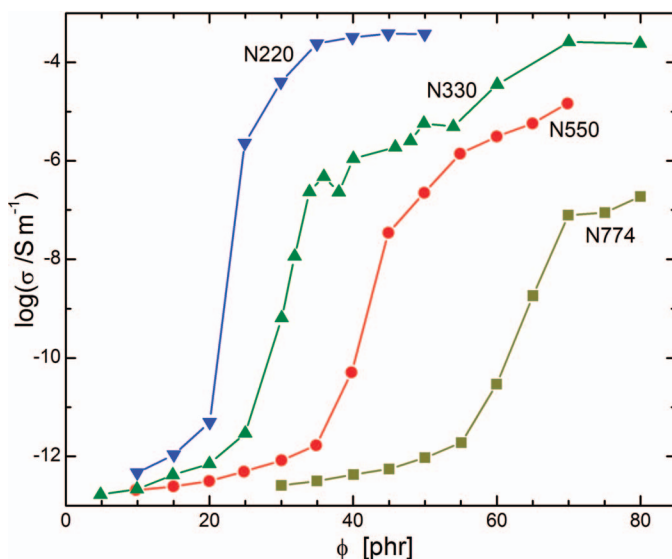
FIG. 4. — dc-Conductivity of SBR copolymer containing various concentrations (parts per hundred rubber) of the indicated carbon black. The steep rise reflects formation of a continuous network of particles. Data from ref 16.

concentration on conductivity to become negligible; however, percolation threshold for this system is significantly less, $\phi^* = 0.38$.[21] Of course, real materials have random packing, rather than body centered, which reduces the number of contacts, thus increasing ϕ^*. The percolation threshold is affected by particle size and shape, the state of dispersion, and the packing geometry. This geometry can be complex, since the conductive pathways are not straight and parallel, but rather meander through the insulating polymer medium.

Figures 5 and 6 illustrate that smaller particles, having higher specific surface areas, will form a percolated network at lower concentrations. This property underlies the appeal of nanoparticles.
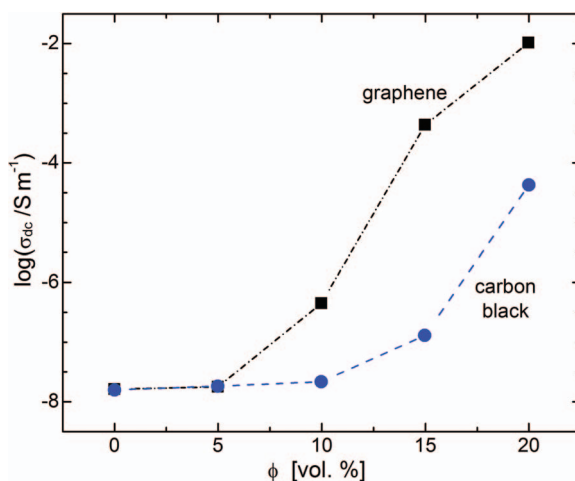

FIG. 5. — Conductivity versus concentration of graphene (squares) and N339 carbon black (circles); the matrix was NBR. Data from ref 22.
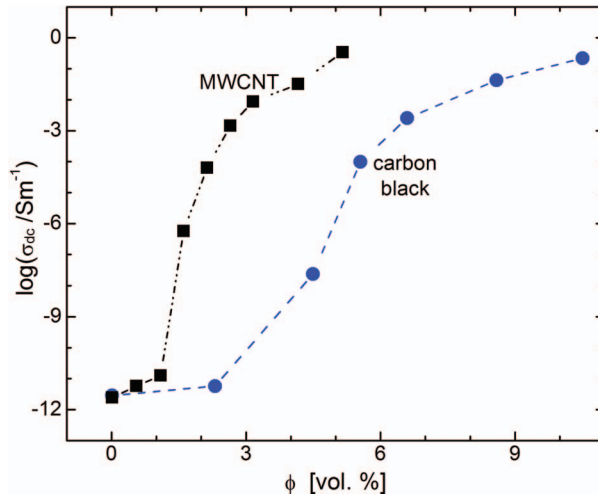
FIG. 6. — Conductivity versus concentration of multiwalled carbon nanotubes (squares) and a high-structure, conductive carbon black (circles); the matrix was SBR. Data from ref 23.

The significantly enhanced conductivity in comparison to carbon black is seen in Figure 5 for graphene[22] and Figure 5 for multiwalled carbon nanotubes.[23]

Figure 7 shows the conductivity as a function of the mean distance between particle surfaces for various loadings of high-abrasion furnace carbon black in NR, the latter determined from analysis of three-dimensional transmission electron microscopy (TEM) images.[24] If the contribution from tunneling is negligible, then the interface between the polymer and filler particles acts as a parallel resistor and capacitor, governed by the relation
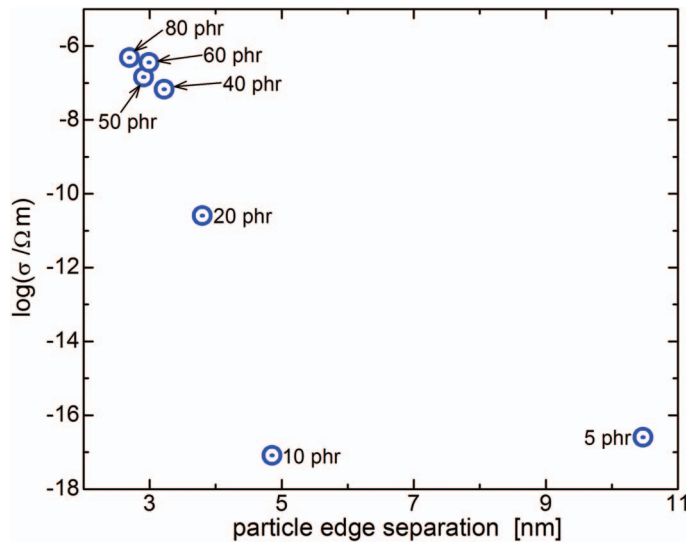
$$R = \tau_{RC}/C \tag{13}$$

FIG. 7. — Conductivity of NR with the indicated concentration of N330 carbon black, as a function of the distance between the particle surfaces (obtained from TEM). Data from ref 24.
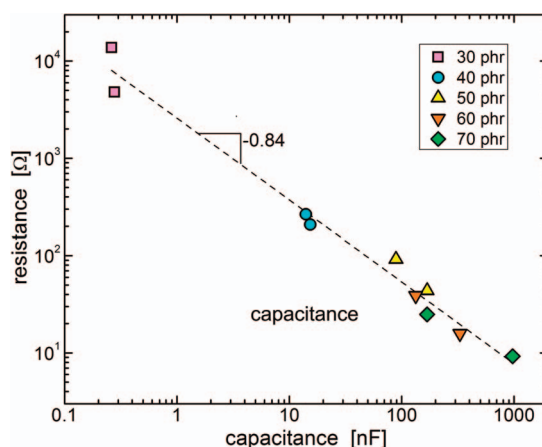
FIG. 8. — Resistance versus capacitance measured for SBR with the indicated concentrations of N234 carbon black. The data deviate from the inverse proportionality expected if the rubber layer at the interface of the carbon particles forms a simple RC circuit, without other mechanisms, such as tunneling, influencing the conduction. Data from ref 25.

in which τ_{RC} is a time constant. Equation 13 implies that the resistance and capacitance should be inversely proportional, which is observed at higher frequencies. In Figure 8 R is plotted versus C for 10 compounds having different levels of carbon black.[25] The approximate inverse proportionality of the two quantities is consistent with gaps between the carbon particles determining both R and C. More detailed modeling would include the tunnel contribution to the observed conductivity.[26]

Particle contacts develop during the dispersion process; thus, electrical conductivity reflects the degree of agglomeration of the particles, including disruption of any network of particles by strain.[27] An important difference between the use of conductivity to assess dispersion and conventional optical or microroughness methods is that the former is determined by the dispersed particles, whereas the latter reflects undispersed or agglomerated particles.[28] Table I compares the dispersion rating based the topography of a cut surface to the conductivity measured for a styrene–butadiene rubber (SBR) copolymer containing a high-structure carbon black.[29] The conductivity continues to show large changes, indicating continued dispersion of the particles, for mixing times for which the dispersion rating has become constant.

The sensitivity of electrical conduction to the particle separation (Figure 7) can be exploited for pressure–sensor applications.[30–32] Figure 9 shows the change in impedance of a carbon black–filled silicone rubber when small tensile forces are applied.[33] The ac-response is larger than the change in dc-conductivity because the former is also affected by the capacitance, which decreases when the material is deformed (Eq. 13). With response and recovery times of a few seconds, the technology holds promise for developing an artificial electronic skin for use in prostheses and wearable medical

TABLE I
COMPARISON OF CARBON BLACK DISPERSION FROM SURFACE TOPOGRAPHY AND ELECTRIC CONDUCTIVITY FOR SBR CONTAINING 55 PHR N347[a]

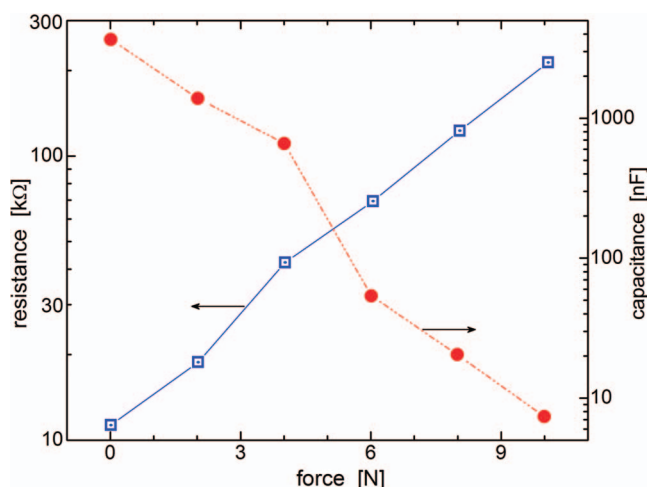| Mixing time, min	2.5	3.0	8.0	12.0	16.0
Dispersion rating	5.8	6	8.3	8.9	8.8
Conductivity, S/m	1.1×10^{-5}	1.3×10^{-5}	3.5×10^{-8}	1.4×10^{-8}	3.7×10^{-9}

[a] From ref 29.

FIG. 9. — Change in the impedance (squares) and capacitance (circles) of a carbon black–filled silicone elastomer measured at 1 kHz as a function of the applied tensile force. Data from ref 33.

devices.[34–37] Generally, elastomers have application as actuators and transducers by converting electrical energy into mechanical work, primarily via electrostriction (Maxwell strain).[38–40]

The labile nature of the interparticle contacts also confers a temperature sensitivity to the conductivity. Interestingly, more stable electrical properties[41] and lower percolation thresholds[42] can be achieved with a phase-separated polymer blend; the mechanism seems to be conductive pathways formed by the filler particles along the domain boundaries. Nonuniform distribution of the filler between the phases of a blend can be used to engineer the electrical properties.[43,44] A novel variation on this approach is to include large (150 nm) silica particles that facilitate dispersion of the carbon black and engender formation of a connected network of the latter; conductivities much larger than those seen in Figure 4 can be obtained.[45] Modification of the surface of carbon nanotubes has been shown to promote strong interaction with the polymer chains, conferring an insensitivity of the electrical conductivity to strain.[46]

As illustrated in Table I, mixing breaks up the agglomerated structure, reducing the conductivity. However, this dispersion is preceded by an initial phase during which σ may rise, as the particles become more uniformly distributed through the polymer matrix. This is seen directly by in situ measurements during mixing (Figure 10).[47,48] For fillers such as carbon nanotubes that are difficult to disperse, the conductivity is mainly observed to increase, since extensive mixing is required to incorporate the particles into the polymer (Figure 11).[49]

B. DYNAMICS OF RUBBER

Since the motions prevailing at equilibrium enable the molecular dipoles to remain unoriented on average, the measured time-dependent fluctuations of the polarization correspond to the equilibrium dynamics. For small molecules (simple liquids) dielectric relaxation spectroscopy probes the molecular reorientations. For most polymers the dipole moment is transverse to the chain, so that the dielectric experiment probes the local segmental dynamics (the α-process) and any higher frequency secondary relaxations due to restricted torsional motions of the chain and any side group dynamics. Figure 12 shows the various dielectric processes observed in 1,4-polybutadiene (BR).[50] At frequencies lower than the local segmental relaxation peak, those few polymers having a dipole moment parallel to the backbone, which means their repeat unit structure lacks a symmetric
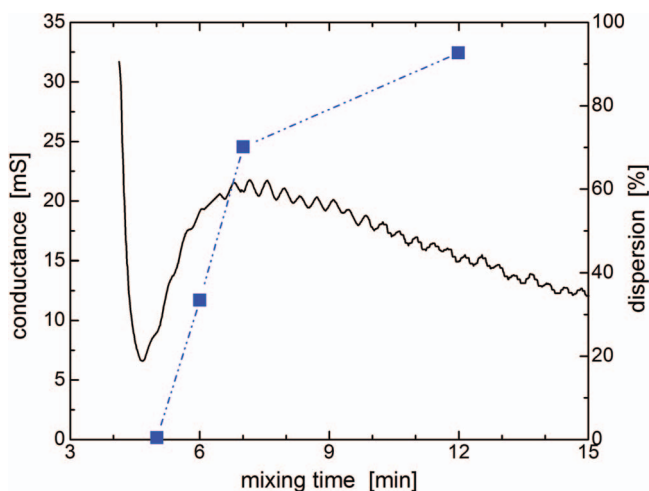
FIG. 10. — Electrical conductance (line) measured in situ during mixing of 50 phr N220 carbon black in SBR; corresponding filler dispersion measured at selected times is indicated by the symbols. Data from ref 47.

center, exhibit a normal mode peak reflective of the end-to-end fluctuations of the chains. This global relaxation process is absent in Figure 12, since polybutadiene has no parallel dipole moment.

1. Local Segmental Dynamics. — The local segmental dynamics corresponds to intra-molecular correlated rotations of a couple of backbone bonds,[51] yielding a segmental relaxation peak invariably broader than the 1.14 decades full width at half maximum of the Debye function

$$\varepsilon^*(\omega) = \varepsilon_\infty + \frac{\Delta\varepsilon}{1 + i\omega\tau_D} \qquad (14)$$

where τ_D is the Debye relaxation time, and $\Delta\varepsilon$ is the dielectric strength ($=\varepsilon_s - \varepsilon_\infty$ where ε_s is the static
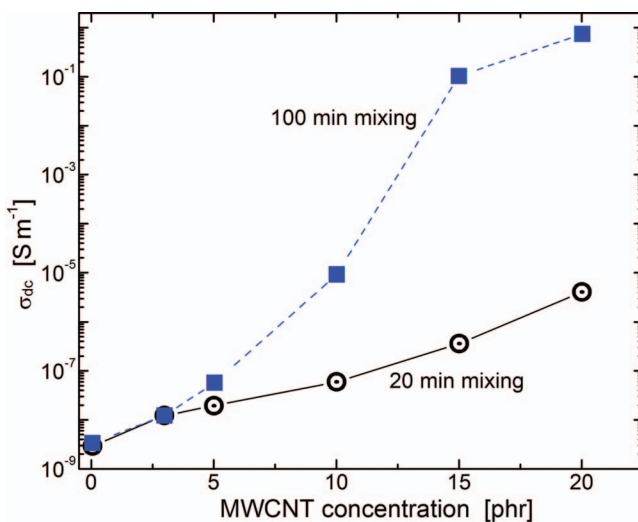

FIG. 11. — Electrical conductivity as function of multiwall carbon nanotube concentration for two durations of mixing. Data from ref 49.
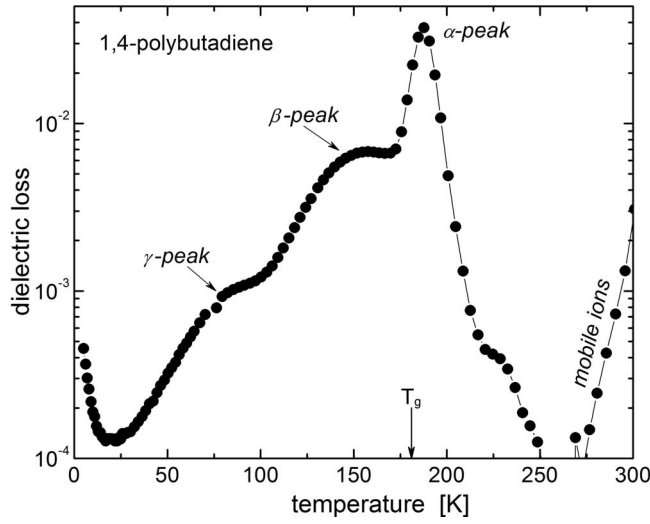
FIG. 12. — Dielectric loss of BR measured at 100 Hz as a function of temperature, with the various dispersions indicated. The arrow denotes the calorimetric T_g. Data from ref 50.

or low-frequency permittivity and ε_∞ is the constant, high-frequency value). The Debye function corresponds in the time domain to exponential decay. Segmental relaxation spectra are usually fit to either the Havriliak–Negami (H-N) equation[11]

$$\varepsilon^*(\omega) = \Delta\varepsilon[1 + (i\omega\tau_{HN})^a]^{-b} \tag{15}$$

where τ_{HN}, a, and b are constants, or the Kohlrausch–Williams–Watts (KWW) function[11]

$$\varepsilon^*(\omega) = \Delta\varepsilon\hat{L}_{i\omega}\left[-\frac{d\varphi(t)}{dt}\right] \tag{16}$$

$$\varphi(t) = \exp\left[-(t/\tau_K)^{\beta_K}\right] \tag{17}$$

with τ_K and β_K as constants, and $\hat{L}_{i\omega}$ denoting the Laplace transform. Equation 15 is empirical, but having three adjustable parameters can be fit to experimental loss peaks for a variety of materials and relaxation processes. Equation 17, which has one fewer adjustable parameter, can be derived in various ways, including from models based on free volume,[52] hierarchal constraints,[53] defect diffusion,[54] defect distances,[55] random free energy,[56] intermolecular cooperativity,[57,58] or molecular weight polydispersity.[59] The KWW function can also be obtained by assuming a particular distribution of exponential decay functions.[9,10] The model-independent relaxation time defined from the inverse of the peak frequency is longer than τ_K and τ_{HN}, the values of which depend on the shape parameters a, b, and β_K.

Figure 13 shows representative dielectric loss spectra of a siloxane polymer measured as a function of both temperature and pressure.[60] A feature almost unique to dielectric spectroscopy is the ability to obtain spectra over broad ranges of temperature and pressure. This has enabled a number of findings, such as the fact that the slowing down of the segmental dynamics as polymers are cooled toward their glass transitions is due primarily to the loss of thermal energy, rather than jamming from the loss of free volume accompanying thermal contraction of the material.[61]
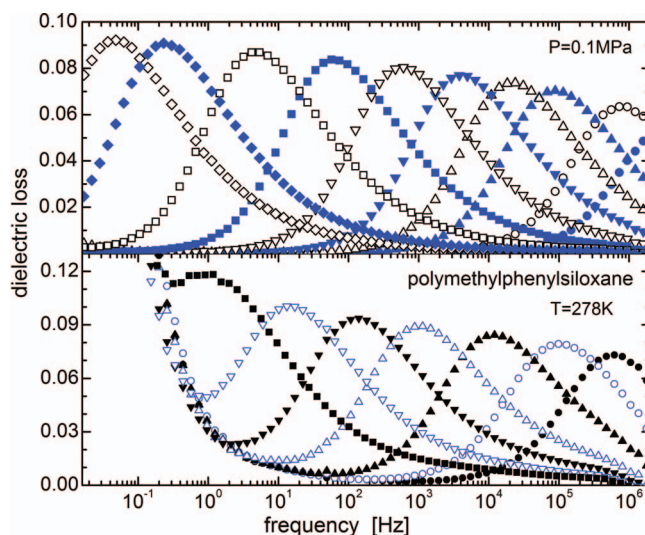
FIG. 13. — Dielectric loss curves for polymethylphenylsiloxane (molecular weight [M_w] = 12.6 kg/mol) as function of (top) temperatures from 247 to 289 K (left to right) and (bottom) pressures from 6 to 112 MPa (right to left). Data from ref 60.

Dielectric relaxation measurements also led to the discovery of density scaling in polymers, whereby for any thermodynamic state point the local segmental relaxation time depends uniquely on the ratio of the temperature to density, with the latter raised to a material constant.[3,62]

Figure 14 shows the dielectric spectra of an elastomeric polyurea (calorimetric T_g = 219 K) measured as a function of uniaxial strain. With increasing deformation, the segmental relaxation peak moves to lower frequencies and broadens.[63] Evidently tensile deformation perturbs the phase-separated structure, causing some interfacial mixing of hard and soft domains, with consequent
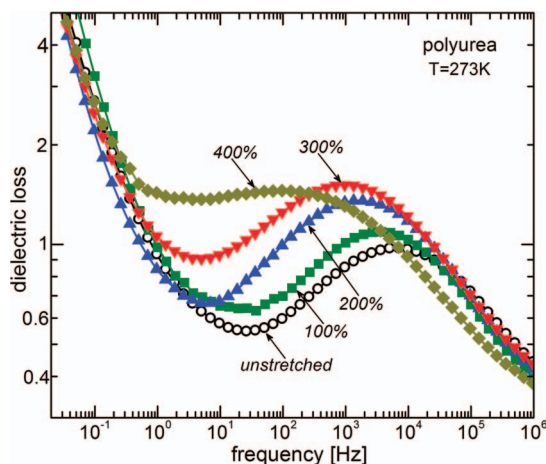

FIG. 14. — Dielectric spectra of polyurea measured under uniaxial deformation of the indicated amounts. With increasing strain, the segmental relaxation peak moves to lower frequencies and broadens. Data from ref 63.
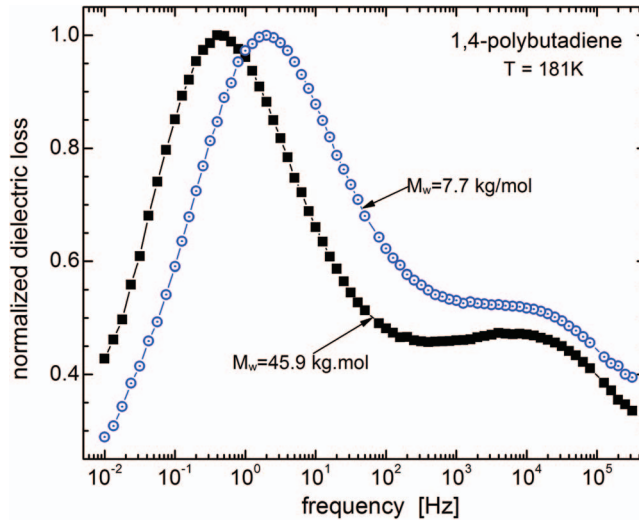
FIG. 15. — Dielectric loss curves for two BR, having the indicated molecular weights. The T_g equals 173.1 K for the lower M_w sample and 174.8 K for the higher M_w sample. The local segmental peak shifts in accord with T_g; however, the higher frequency J-G peak position is independent of molecular weight. Data from ref 66.

slowing down and broadening of the soft phase segmental dynamics. This effect is not seen in analogous experiments on a homogeneous polymer such as polyisoprene.[64]

2. Secondary Relaxations. — Secondary relaxations in polymers occur at higher frequencies than the segmental dynamics, and they are often fit using the symmetric Cole–Cole function[11]

$$\varepsilon^*(\omega) = \frac{\Delta\varepsilon}{1 + (i\omega\tau_{CC})^{1-\gamma}} \tag{18}$$

where γ and τ_{CC} are constants. Equation 18 corresponds to the H-N function (Eq. 15) with $b=1$, and reduces to the Debye function (Eq. 14) for $\gamma = 0$. There are two types of secondary processes. The most common involves pendant moieties or a group of atoms in a bulky chain molecule. These secondary relaxations are almost unique to polymers, and they have no particular relationship to the glass transition. The other type of secondary process, the so-called Johari–Goldstein (J-G) relaxation, involves the entire repeat group in the polymer.[65] The J-G relaxation usually has weaker intensity than the segmental peak because the amplitude of the J-G motion is more limited.

Figure 15 shows the dielectric relaxation spectra for BR. There is a prominent secondary relaxation falling close to the segmental relaxation peak.[66] If the peaks are well separated, the relaxation times can be obtained by fitting the spectra with the assumption that the α- and J-G contributions are additive. If the two peaks are close, this assumption may break down, depending on the relative intensities. An alternative procedure is to use an equation from Williams[67]

$$\varepsilon(t) = f_\alpha\varepsilon_\alpha(t) + (1 - f_\alpha)\varepsilon_\beta(t) \tag{19}$$

that assumes the secondary relaxation transpires in an environment rearranging on the timescale of the α-dynamics. Note that J-G peaks are generally very weak or absent in the corresponding mechanical spectra, since their motion does not perturb significantly the local density.

3. Coupling of Relaxation and Ionic Conductivity. — The conductivity due to mobile ions is usually coupled to the reorientational dynamics, since motion of the chain segments provides
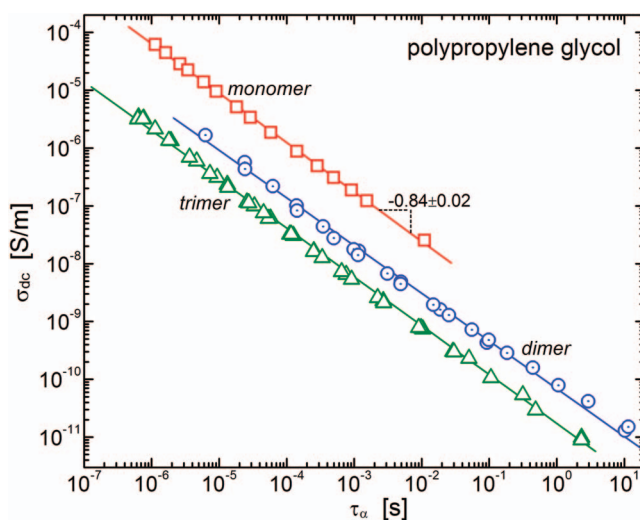
FIG. 16. — Conductivity vs α-relaxation time for propylene glycol monomer, dimer, and trimer at various temperatures and pressure. Best power-law fit yields $j = 0.84 \pm 0.02$ for all three liquids. Data from ref 70.

diffusive pathways for the ions. This coupling is not observed for electrical conduction. An empirical relation[68]

$$\sigma_{dc}\tau_\alpha^j = \text{const} \qquad (20)$$

is used to correlate the conductivity and segmental relaxation, with the exponent j from Eq. 4. This slaving of the conductivity to the chain dynamics can be an issue in the use of polymers as exchange membranes, for example, in photovoltaic devices and fuel cells, because increasing the ion conductivity by lowering T_g comes at the expense of mechanical stability.[69] Figure 16 shows double logarithmic plots of σ_{dc} versus τ_α for propylene glycol monomer, dimer, and trimer[70]; the data conform to Eq. 20 with the same slope ($j = 0.84 \pm 0.02$) for the three molecular weights. The magnitude of the conductivity, however, increases with molecular weight.

4. Normal Mode Relaxation. — Polymers having a component of their dipole moment parallel to the chain contour exhibit a so-called normal mode peak, reflecting fluctuations of the chain end-to-end vector.[71,72] These polymers are referred to as having type-A dipoles (or being type-A polymers), whereas dipole moments transverse to the chain backbone are known as type-B dipoles. Polymers with dielectrically active normal modes that have been measured are listed in Table II.[73–84] As noted from their structures, the requirement is that the chain lacks an inversion center; consequently, the dipoles for each segment add vectorially to yield the end-to-end vector measured in the dielectric experiment. As an example, vinyl polymers such as polyvinylchloride have no dielectric normal mode because there is an inversion center (actually two, on both the methylene- and the vinyl-substituted carbons). An exception to this structural requirement is helically configured polymer chains; these chains can exhibit a normal mode peak in their dielectric spectrum even when their repeat units have inversion symmetry; polysulfones provide an example of this behavior.[85,86]

Representative spectra having normal mode peaks are shown in Figure 17.[77] All type-A polymers also possess type-B dipoles, so there is both a normal mode peak and segmental relaxation peak in the spectra. Sometimes referred to as the global relaxation, the normal mode peak falls at lower frequencies than the local segmental dispersion, by an amount supralinear in the polymer molecular weight.[3] For this reason there is greater separation of the two relaxation processes for

TABLE II
POLYMERS HAVING DIELECTRICALLY ACTIVE NORMAL MODES

Polymer	Ref	Repeat structure
Polyisoprene	73	
Polychloroprene	74	
Polybromoprene	75	
Polypropylene oxide	76,77	
Polyoxybutylene	77	
Polystyrene oxide	78	
Poly(alkyl glycidyl ether)	79	
Polydichloro-1,4-phenylene oxide	80	
Polylactide, polylactone	81,82	
Polyphosphazene	83	
Polyphenylacetylene	84	

higher molecular weight materials (Figure 18).[73] Nevertheless, most dielectric studies of normal mode polymers involve measurements of low M_w samples, so that the normal mode peak is not subsumed by intense dc-conductivity at low frequencies.

At high temperatures the two relaxation processes have equivalent T-dependences, whereas at temperatures approaching the glass transition, the normal mode relaxation time is less sensitive to temperature than the more local α-process.[87] Similarly, the pressure dependence of the normal mode is weaker than that of the segmental dynamics. Thus, the two dispersions tend to merge for larger values of the relaxation times, as seen in Figure 18.[73]

5. *Nonlinear Measurements*. — The magnitude of the electric fields used in the dielectric experiments described above is small. This means that the polarization energy resulting from dipole orientations induced by the field is less than the available thermal energy; that is, $\mu E << kT$, where the field E is the gradient of the electric potential and k is the Boltzmann constant. The orientation is transient, never exceeding in magnitude that due to Brownian occurring in the absence of the field. Accordingly, the time-varying current measured in a linear dielectric relaxation experiment
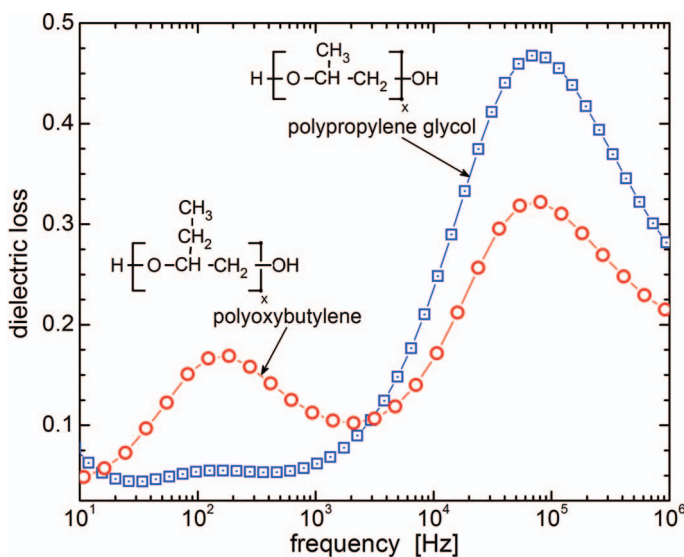
FIG. 17. — Dielectric loss spectra of PPG (squares) and POB (circles) having the same degree of polymerization (=67), measured at conditions (T =293 K and P = 616 MPa for PPG; T = 297 K and P = 351 MPa for PBO) for which the peak frequencies are nearly equal (∼150 Hz for the normal mode and ∼80 kHz for the segmental relaxation). Data from ref 77.

corresponds to the decay of spontaneous thermal fluctuations prevailing at equilibrium; therefore, the linear time correlation function describing the dynamics can be obtained.

At temperatures near the glass transition, the dynamics of liquids and polymers becomes much slower, reflected in large increases in viscosities and relaxation times.[3,61] This slowing down of the molecular and segmental dynamics is a consequence of growing cooperativity, as motion of a molecule or segment increasingly requires adjustments of neighboring species; that is, the motions exert reciprocal influences.[88] Quantification of these space–time correlations is essential to understanding the dynamic properties of liquids and polymers close to T_g. However, a linear time correlation function only provides information about a quantity (e.g., dipole moment or local density) at two times, but characterizing dynamic correlations requires information about the orientation or density simultaneously at two positions and two times. Specifically, the spatial extent of the fluctuations are described by the four-point correlation function[89]

$$\chi_4(t) = \int \langle \rho(r_1, 0)\rho(r_1 + r_2, 0)\rho(r_1, t)\rho(r_1 + r_2, t)\rangle_{r_1} dr_2 \qquad (21)$$

where $\chi_4(t)$ gives the probability that if correlation between two species is lost over a time span t at position r_1, the same decorrelation transpires within this time interval at r_2. The correlation volume, V_{corr}, is proportional to the maximum value of $\chi_4(t)$, which occurs in the vicinity of $t = \tau_\alpha$

$$V_{corr} \propto \max\{\chi_4(t)\} \approx \chi_4(\tau_\alpha) \qquad (22)$$

This higher order function thus quantifies dynamic correlations. Unfortunately, $\chi_4(t)$ cannot be measured by linear relaxation spectroscopy, although estimates can be obtained by making certain assumptions.[90,91]

Based on the idea that higher order correlation functions should be connected to higher order susceptibilities, however, Bouchaud and Biroli[92] derived an expression for $\chi_4(t)$ in terms of the third-order nonlinear susceptibility χ_3
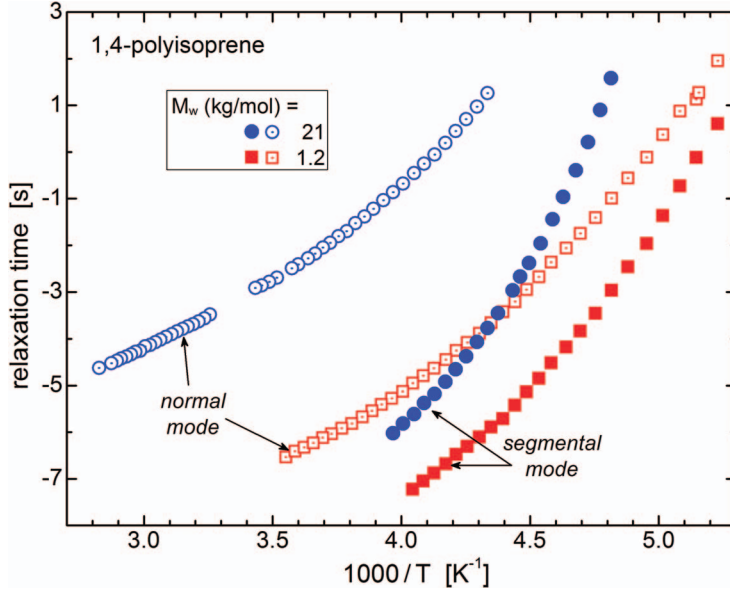
FIG. 18. — Local segmental (filled symbols) and normal mode (open symbols) relaxation times for two polyisoprenes having the indicated molecular weights. The separation of the local and global response increases with increasing chain length. Data from ref 73.

$$V_{cor} \propto |\chi_3| \frac{kT}{\varepsilon_0 a^3 (\Delta\varepsilon_1)^2} \tag{23}$$

where a the molecular or repeat unit volume, and $\Delta\varepsilon_1$ refers to the linear dielectric strength. $|\chi_3|$ is the modulus of the susceptibility corresponding to polarization cubic in the applied field, measured at 3ω, where ω is the frequency of the field. Equation 23 indicates that dynamic correlations make a contribution to the nonlinear susceptibility, so that χ_3 enables V_{corr} to be determined. Nonlinear dielectric experiments require samples with large dipole moments and the application of large electric fields. However, this means the condition $\mu E \ll kT$ is no longer met, and hence nontransient orientation of the dipoles also makes a contribution to the measured spectra.

This dipole orientation contribution saturates at low frequencies ($\omega\tau_\alpha < 1$), where the molecular orientation follows the electric field. This saturation effect can be subtracted from the χ_3 spectrum by calculating the orientation contribution. With the assumption the dipoles are rigid and independent[93,94]

$$\chi_3^{sat}(\omega) = \frac{-3\varepsilon_0 a^3 (\Delta\chi_1)^2}{5kT} \int_0^\infty g(\tau) \frac{3 - 17\omega^2\tau_0^2 + i\omega\tau_0(14 - 6\omega^2\tau_0^2)}{(1 + \omega^2\tau_0^2)(9 + 4\omega^2\tau_0^2)(1 + 9\omega^2\tau_0^2)} d\tau \tag{24}$$

In this expression, $g(\tau)$ is the distribution of relaxation times. Using the H-N distribution underlying Eq. 15 for $g(\tau)$,[95] results are shown in Figure 19 for propylene carbonate.[96] After subtraction of χ_3^{sat} from the measured spectrum, the resulting peak provides a measure of the correlation volume (Eq. 23). To date, this method has only be used to measure V_{corr} for materials with large dipole moments,[96–98] and it has not yet been applied to polymers.
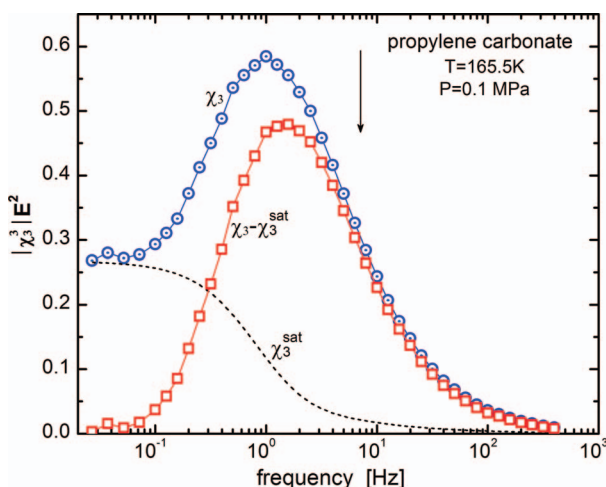
FIG. 19. — Third-order harmonic spectrum of propylene carbonate as measured (circles) and after subtraction of the dipole saturation effect (Eq. 24; squares). The dipole saturation, indicated by the dashed line, decays rapidly with increasing frequency. The peak electric field in this experiment was 11.3 MV/m. Spectra are plotted times the squared field to make these quantities, which describe polarization cubic in the field, comparable to the linear susceptibility, which refers to polarization proportional to E; that is, $\chi_{\text{total}} = \chi_1 + \chi_3 E^2$. The arrow denotes the frequency of the peak in the linear dielectric spectrum. Data from ref 96.

IV. SUMMARY

Impedance spectroscopy and dielectric relaxation experiments use similar instrumentation, but they are used for different purposes. Impedance spectroscopy, in particular dc-conductivity measurements, is applied to polymer composites most often to assess the dispersion and state of aggregation of conductive fillers. In dielectric spectroscopy the usual objective is determination of the dipole reorientation dynamics that underlies, for example, structural relaxation and the glass transition of polymers. Contributions to the spectra from dc-conductivity interfere with the measurement of relaxation peaks. Thus, spectral features that comprise the main interest of impedance spectroscopy are mainly complications in relaxation studies. Although almost all dielectric relaxation experiments are carried out in the linear regime, yielding time correlation functions, there has been recent interest in the use of large electric fields to modify the permittivity. The objective is to measure high-order susceptibilities, which are possibly connected to higher order, dynamic correlation functions.

V. ACKNOWLEDGEMENT

VI. REFERENCES

[1] K. Kessairi, S. Napolitano, S. Capaccioli, P. Rolla, and M. Wubbenhorst, *Macromolecules* **40**, 1786 (2007).

[2] K. Kunal, M. Paluch, C. M. Roland, J. E. Puskas, Y. Chen, and A. P. Sokolov, *J. Polym. Sci. Polym. Phys.* **46**, 1390 (2008).

[3] C. M. Roland, *Viscoelastic Behavior of Rubbery Materials*, Oxford University Press, Oxford, UK, 2011.

[4] R. Diaz-Calleja and E. Riande, *Mater. Sci. Eng. A* **370**, 21 (2004).

[5]N. G. McCrum, B. E. Reed, and G. Williams, *Anelastic and Dielectric Effects in Polymeric Solids*, Wiley, New York, 1967.

[6]U. Buchenau, M. Ohl, and A. Wischnewski, *J. Chem. Phys*. **124**, 094505 (2006).

[7]J. Colmenero, A. Alegria, P. G. Santangelo, K. L. Ngai, and C. M. Roland, *Macromolecules* **27**, 407 (1994).

[8]A. A. Pronin, M. V. Kondrin, A. G. Lyapin, V. V. Brazhkin, A. A. Volkov, P. Lunkenheimer, and A. Loidl, *Phys. Rev. E* **81**, 041503 (2010).

[9]C. P. Lindsey and G. D. Patterson, *J. Chem. Phys*. **73**, 3348 (1980).

[10]M. N. Berberan-Santos, E. N. Bodunov, and B. Valeur, *Chem. Phys*. **315**, 171 (2005).

[11]*Broadband Dielectric Spectroscopy*, F. Kremer and A. Schonhals, Eds., Springer-Verlag, Berlin, 2003.

[12]R. Richert, *J. Non Cryst. Solids* **172–174**, 209 (1994).

[13]M. Wubbenhorst and J. van Turnhout, *J. Non Cryst. Solids* **305**, 40 (2002).

[14]M. L. Jimenez, F. J. Arroyo, J. van Turnhout, and A. V. Delgado, *J. Coll. Interface Sci*. **249**, 327 (2002).

[15]R. Casalini and C. M. Roland, *J. Polym. Sci. Polym. Phys. Ed*. **48**, 582 (2010).

[16]C. P. O'Farrell, M. Gerspacher, and L. Nikiel, *Rubber Plast. News*, July 1999, p 71.

[17]R. Holm, *Electric Contacts*, Springer, Berlin, 1967.

[18]C. Sun, P. Zhang, C. Wrana, R. Schuster, and S. Zhao, RUBBER CHEM. TECHNOL. **87**, 647 (2014).

[19]G. A. Schwartz, S. Cerveny, A. J. Marzocca, M. Gerspacher, and L. Nikiel, *Polymer* **44**, 7229 (2003).

[20]A. I. Medalia, RUBBER CHEM. TECHNOL. **59**, 432 (1986).

[21]G. R. Ruschau, S. Yoshikawa, and R. E. Newnham, *J. Appl. Phys*. **72**, 953 (1992).

[22]M. M. Mowes, F. Fleck, and M. Kluppel, RUBBER CHEM. TECHNOL. **87**, 70 (2014).

[23]L. Bokobza, *Vib. Spectrosc*. **51**, 52 (2009).

[24]A. Kato, J. Shimanuki, S. Kohjiya, and Y. Ikeda, RUBBER CHEM. TECHNOL. **79**, 653 (2006).

[25]L. C. Burton, K. Hwang, and T. Zhang, *Rubber Chem. Technol*. **62**, 838 (1989).

[26]Z. Xie, Y.-J. Yum, H.-G. Min., and J.-H. Son, *Mater. Sci. Forum* **575–578**, 930 (2008).

[27]C. M. Roland and G. F. Lee, RUBBER CHEM. TECHNOL. **63**, 554 (1990).

[28]L. Guerbe and P. K. Freakley, *Kaut. Gummi Kunst*. **48**, 260 (1995).

[29]R. J. Cembrola, *Polym. Eng. Sci*. **22**, 601 (1982).

[30]J. Zavickis, M. Knite, G. Podins, A. Linarts, and R. Orlovs, *Sens. Actuators A Phys*. **171**, 38 (2011).

[31]W. Luheng, D. Tianhuai, and W. Peng, *Sens. Actuators A Phys*. **135**, 587 (2007).

[32]K. Yoshimura, K. Nakano, K. Okamoto, and T. Miyake, *Sens. Actuators A Phys*. **180**, 55 (2012).

[33]H. Mei, C. Zhang, R. Wang, J. Feng, and T. Zhang, *Sens. Actuators A Phys*. **233**, 118 (2015).

[34]L. Pan, A. Chortos, G. Yu, Y. Wang, S. Isaacson, R. Allen, Y. Shi, R. Dauskardt, and Z. Bao, *Nat. Commun*. **5**, 3002 (2014).

[35]D. J. Lipomi, M. Vosgueritchian, B.C.-K. Tee, S. L. Hellstrom, J. A. Lee, C. H. Fox, and Z. Bao, *Nat. Nanotechnol*. **6**, 788 (2011).

[36]D.-H. Kim, N. Lu, R. Ma, Y.-S. Kim, R.-H. Kim, S. Wang, J. Wu, S. M. Won, H. Tao, A. Islam, K. J. Yu, T. Kim, R. Chowdhury, M. Ying, L. Xu, M. Li, H.-J. Chung, H. Keum, M. McCormick, P. Liu, Y.-W. Zhang, F. G. Omenetto, Y. Huang, T. Coleman, J. A. Rogers, *Science* **333**, 838 (2011).

[37]X. Wang, Y. Gu, Z. Xiong, Z. Cui, and T. Zhang, *Adv. Mater*. **26**, 1336 (2014).

[38]L. Liu, J. Li, Y. Liu, J. Leng, J. Zhao, and J. Zhao, *J. Mech. Sci. Technol*. **29**, 109 (2015).

[39]R. Shankar, A. K. Krishnan, T. K. Ghosh, and R. J. Spontak, *Macromolecules* **41**, 6100 (2008).

[40]C. M. Roland, J. T. Garrett, R. Casalini, D. F. Roland, P. G. Santangelo, and S. B. Qadri, *Chem. Mater*. **16**, 857 (2004).

[41]J. Zhou, Y. Song, Q. Zheng, X. Jiang, and B. Shui, *J. Appl. Polym. Sci*. **107**, 3083 (2008).

[42]K. M. N. Gamboa, A. J. B. Ferreira, S. S. Camargo, and B. G. Soares, *Polym. Bull*. **38**, 95 (1997).

[43]S. Hom, A. R. Bhattacharyya, R. A. Khare, A. R. Kulkarni, M. Saroop, and A. Biswas, *Polym. Eng. Sci*. **49**, 1502 (2009).

[44]P. Dey, K. Naskar, B. Dash, S. Nair, G. Unnikrishnan, and G. B. Nando, *RSC Adv*. **5**, 31886 (2015).

[45]E. S. Bhagavatheswaran, M. Parsekar, A. Das, H. H. Le, S. Wiessner, K. W. Stöckelhuber, G. Schmaucks, and G. Heinrich, *J. Phys. Chem. C* **119**, 21723 (2015)

[46]K. Guo, D.-L. Zhang, X.-M. Zhang, J. Zhang, L.-S. Ding, B.-J. Li, and S. Zhang, *Angew. Chem. Int. Ed. Engl.* **54**, 12127 (2015).

[47]H. H. Le, Z. Qamer, S. Ilisch, and H.-J. Radusch, RUBBER CHEM. TECHNOL. **79**, 621 (2006).

[48]H. H. Le, E. Hamann, S. Ilisch, G. Heinrich, and H.-J. Radusch, *Polymer* **55**, 1560 (2014).

[49]H. H. Le, X. T. Hoang, A. Das, U. Gohs, K.-W. Stoeckelhuber, R. Boldt, G. Heinrich, R. Adhikari, and H.-J. Radusch, *Carbon* **50**, 4543 (2012).

[50]M. J. Schroeder, K. L. Ngai, and C. M. Roland, *J. Polym. Sci. Polym. Phys.* **45**, 342 (2007).

[51]C. K. Hall and E. Helfand, *J. Chem. Phys.* **77**, 3275 (1982).

[52]M. H. Cohen and G. S. Grest, *Phys. Rev. B* **24**, 4091 (1981).

[53]R. G. Palmer, D. L. Stein, E. Abrahams, and P. W. Anderson, *Phys. Rev. Lett.* **53**, 958 (1984).

[54]J. T. Bendler and M. F. Shlesinger, *Macromolecules* **18**, 591 (1985).

[55]J. Klafter and A. Blumen, *Chem. Phys. Lett.* **119**, 377 (1985).

[56]C. DeDominicis, H. Orland, and F. Lainee, *J. Phys. Lett.* **46**, L463 (1985).

[57]K. L. Ngai, R. W. Rendell, A. K. Rajagopal, and S. Teitler, *Ann. NY Acad. Sci.* **484**, 150 (1986).

[58]M. M. Kubat, P. Riha, R. W. Rychwalski, and S. Uggla, *Mech. Time Depend. Mater.* **3**, 31 (1999).

[59]P.-G. de Gennes, *Macromolecules* **35**, 3785 (2002).

[60]S. Pawlus, S. J Rzoska, J. Ziolo, M. Paluch, and C. M. Roland, RUBBER CHEM. TECHNOL. **76**, 1106 (2003).

[61]C. M. Roland, RUBBER CHEM. TECHNOL. **85**, 313 (2012).

[62]C. M. Roland, S. Hensel-Bielowka, M. Paluch, and R. Casalini, *Rep. Prog. Phys.* **68**, 1405 (2005).

[63]T. Choi, D. Fragiadakis, C. M. Roland, and J. Runt, *Macromolecules* **45**, 3581 (2012).

[64]H. K. Lee, D. Fragiadakis, D. Martin, A. Milne, J. Milne, and J. Runt, *Macromolecules* **43**, 3125 (2010).

[65]K. L. Ngai and M. Paluch, *J. Chem. Phys.* **120**, 857 (2004).

[66]R. B. Bogoslovov, T. E. Hogan, and C. M. Roland, *Macromolecules* **43**, 2904 (2010).

[67]G. Williams, *Adv. Polym. Sci.* **33**, 59 (1979).

[68]S. Corezzi, E. Campani, P. A. Rolla, S. Capaccioli, and D. Fioretto, *J. Chem. Phys.* **111**, 9343 (1999).

[69]R. Casalini, B. L. Chaloux, C. M. Roland, and H. L. Ricks-Laskoski, *J. Phys. Chem. C* **118**, 6661 (2014).

[70]R. Casalini and C. M. Roland, *J. Chem. Phys.* **119**, 11951 (2003).

[71]H. Watanabe, *Macromol. Rapid Commun.* **22**, 121 (2001).

[72]K. Adachi and T. Kotaka, *Prog. Polym. Sci.* **18**, 585 (1993).

[73]D. Fragiadakis, R. Casalini, R. B. Bogoslovov, C. G. Robertson, and C. M. Roland, *Macromolecules* **44**, 1149 (2011).

[74]K. Adachi and T. Kotaka, *Macromolecules* **18**, 294 (1985)

[75]V. P. Petrosyan and Sh. T. Yogurtdzhyan, *Polym Sci. USSR* **9**, 2787 (1967).

[76]J. Mijovic and J.-W. Sy, *J. Non Cryst. Solids* **307–310**, 679 (2002).

[77]R. Casalini and C. M. Roland, *Macromolecules* **38**, 1779 (2005).

[78]Y. Hirose and K. Adachi, *Polymer* **46**, 1913 (2005).

[79]M. Yamane, Y. Hirose, and K. Adachi, *Macromolecules* **38**, 10686 (2005).

[80]K. Adachi and T. Kotaka, *Macromolecules* **16**, 1936 (1983).

[81]M. Mierzwa, G. Floudas, J. Dorgan, D. Knauss, and J. Wegner, *J. Non Cryst. Solids* **307–310**, 296 (2002).

[82]O. Urakawa, K. Adachi, T. Kotaka, Y. Takemoto, and H. Yasuda, *Macromolecules* **27**, 7410 (1994).

[83]S. Uzaki, K. Adachi, and T. Kotaka, *Macromolecules* **21**, 153 (1988).

[84]A. M. North and P. J. Phillips, *Trans. Faraday Soc.* **64**, 3235 (1968).

[85]R. H. Cole, P. Winsor, A. H. Fawcett, and S. Fee, *Macromolecules* **20**, 157 (1987).

[86]A. H. Fawcett and K. J. Ivin, *Polymer* **16**, 569 (1975).

[87]C. M. Roland, K. L. Ngai, P. G. Santangelo, X. H. Qiu, M. D. Ediger, and D. J. Plazek, *Macromolecules* **34**, 6159 (2001).

[88]*Dynamical Heterogeneities in Glasses, Colloids, and Granular Media*, L. Berthier, G. Biroli, J.-P. Bouchaud, L. Cipelletti, and W. van Saarloos, Eds., Oxford University Press, Oxford, UK, 2011.

[89]C. Toninelli, M. Wyart, L. Berthier, G. Biroli, and J.-P. Bouchaud, *Phys. Rev. E* **71**, 041505 (2005).

[90]S. Capaccioli, G. Ruocco, and F. Zamponi, *J. Phys. Chem. B* **112**, 10652 (2008).

[91]D. Fragiadakis, R. Casalini, and C. M. Roland, *J. Phys. Chem. B* **113**, 13137 (2009).

[92]J.-P. Bouchaud and G. Biroli, *Phys. Rev. B* **72**, 064204 (2005).

[93]C. Crauste-Thibierge, C. Brun, F. Ladieu, D. L'Hôte, G. Biroli, and J. P. Bouchaud, *Phys. Rev. Lett*. **104** 165703 (2010).

[94]R. Richert, *Phys. Rev. E* **88**, 062313 (2013).

[95]R. Zorn, *J. Polym. Sci. Polym. Phys. Ed*. **37**, 1043 (1999).

[96]R. Casalini, D. Fragiadakis, and C. M. Roland, *J. Chem. Phys*. **142**, 064054 (2015).

[97]Th. Bauer, M. Michl, P. Lunkenheimer, and A. Loidl, *J. Non Cryst. Solids* **407**, 66 (2015).

[98]C. Brun, F. Ladieu, D. L'Hote, M. Tarzia, G. Biroli, and J.-P. Bouchaud, *Phys. Rev. Lett*. **109**, 175702 (2012).